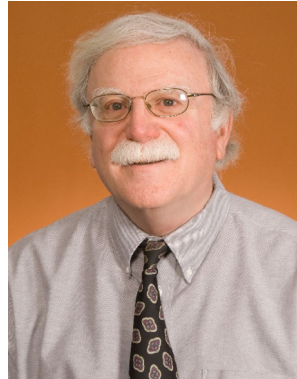


Magnetic Transformations and Phase Diagrams



DAVID E. LAUGHLIN 



DAVID E. LAUGHLIN

When magnetic phases are included on phase diagrams some unfamiliar features appear. Most magnetic transformations are not first-order phase transformations and therefore their depictions on phase diagrams do not have to follow the well-known construction requirements such as those based on the Gibbs Equilibrium Phase Rule. In particular, the transformation from a paramagnetic to ferromagnetic phase should be designated differently than those of the more widely known first-order transformations. The transformation curve (Curie curve) does not display a two-phase equilibrium: rather it shows the limit of stability of the disordered (paramagnetic) phase. In this paper, various examples of phase diagrams which include such *transformations* will be presented and discussed. The role of externally applied magnetic fields will be presented based on fundamental thermodynamic principles and the role that applied magnetic fields play in changing the degrees of freedom of systems (alloys) will be discussed.

<https://doi.org/10.1007/s11661-019-05214-z>

© The Minerals, Metals & Materials Society and ASM International 2019

I. INTRODUCTION: PHASE DIAGRAMS, PHASES, AND PHASE TRANSFORMATIONS

PHASE diagrams are important items in the toolbox of metallurgists and materials scientists. Phase diagrams indicate which phases are in equilibrium under the specific thermodynamic conditions in which a material (the system) may find itself. A phase can be defined as: "...a physically distinct homogeneous portion of a thermodynamic system delineated in space by a bounding surface, called an interphase interface, and distinguished by its state of aggregation (solid, liquid or gas), crystal structure, composition and/degree of order. Each phase in a material system generally exhibits a characteristic set of physical, mechanical and chemical properties and is, in principle, mechanically separable from the whole."^[1] When the thermodynamic conditions change, a phase may transform into one or more different phases. Phase diagrams designate the thermodynamic conditions that accompany such phase changes.

Simple unary systems are those that are closed to changes in composition and whose state is determined by

DAVID E. LAUGHLIN is the ALCOA Professor of Physical Metallurgy Materials Science and Engineering, Carnegie Mellon University, Pittsburgh, PA 15213. Contact e-mail: Laughlin@cmu.edu

David E. Laughlin is Professor in the Materials Science and Engineering Department, Carnegie Mellon University, where he has been on the Faculty since 1974. He also holds a Courtesy Appointment in the Electrical and Computer Engineering Department at CMU. David is a graduate of Drexel University (BS in Metallurgical Engineering, 1969) and Massachusetts Institute of Technology, Ph.D. in Metallurgy, 1973). He was the Principal Editor of the *Metallurgical and Materials Transactions* family of journals of ASM International and TMS from 1987 to 2016. David has been a Leader in the Data Storage Systems Center Magnetic Recording Group since 1989. He has taught courses on physical metallurgy, electron microscopy, diffraction techniques, thermodynamics, crystallography, magnetic materials, phase transformations, and ferroic materials. David has more than 400 technical publications and is the Editor (with Hiro Hono) of the three volume *Physical Metallurgy* (Elsevier). He also is the Author (with David Gaskell), of the 6th edition of *Introduction to the Thermodynamics of Materials*. David is an Honorary Member of the AIME and is a Fellow of ASM International and TMS.

Manuscript submitted December 20, 2018.

Article published online April 16, 2019

two independent thermodynamic variables, usually taken as the temperature and pressure. Such systems have three possible regions of phase stability in their two-dimensional pressure–temperature phase diagrams:

- *Areas*, in which one phase is present with two thermodynamic degrees of freedom.
- *Curves*, on which two phases are in thermodynamic equilibrium, having one thermodynamic degree of freedom.
- *Points*, at which three phases are in thermodynamic equilibrium with no thermodynamic degrees of freedom.

In such simple unary systems, the thermodynamic energy potentials and their natural independent variables are

$$\text{Internal energy: } U = U(S, V), \quad [1a]$$

$$\text{Enthalpy: } H = H(S, P), \quad [1b]$$

$$\text{Helmholtz free energy: } A = A(T, V), \quad [1c]$$

$$\text{Gibbs free energy: } G = G(T, P). \quad [1d]$$

When an additional independent *intensive field*, such as the magnetic field, \mathcal{H} , is present, a three-dimensional phase diagram which has the three intensive variables as its axes (P , T , and \mathcal{H}) may have the following stability regions:

- Three-dimensional regions, in which one phase is present with three degrees of thermodynamic freedom.
- Two-dimensional surfaces, on which two phases are in thermodynamic equilibrium having two thermodynamic degrees of freedom.
- Curves, on which three phases are in thermodynamic equilibrium with one thermodynamic degree of freedom.
- Points, at which four phases may exist in thermodynamic equilibrium with no thermodynamic degree of freedom.

For such systems, one can write the functional form of the Gibbs free energy as follows:

$$G = G(T, P, \mathcal{H}). \quad [1e]$$

The conjugate thermodynamic variable to the intensive magnetic field is the magnetization M , which is also referred to as the order parameter of the ferromagnetic phase.

When materials are composed of more than one chemical component, additional *intensive variables* are introduced, known as the *chemical potentials*. When Φ phases are in equilibrium, the chemical potential of each component is the same in each of the Φ phases. If the chemical potentials are not the same, a driving force exists for diffusion of the components among the phases.

When metallurgists or materials scientists are introduced to phase diagrams, the diagrams are usually the ones in which the various phase transformations are *first-order phase transformations*. Indeed the above description of the 2-D and 3-D phase diagrams assumes that the boundaries between phase regions are first-order boundaries at which the phases on either side of the boundaries are in equilibrium coexistence. Certain geometrical conditions are imposed on the diagrams of first-order transformations, one of which is summarized in the Gibbs Equilibrium Phase Rule:

$$\Phi + \mathcal{F} = C + \mathcal{X}. \quad [2]$$

Here, Φ is the number of phases which may be present, C is the number of components, \mathcal{X} is the number of independent intensive variables (or fields) on the system, and \mathcal{F} is the number of degrees of freedom. For example, for a simple unary system with pressure and temperature as the intensive field variables:

$$\Phi + \mathcal{F} = 3.$$

This limits the number of possible phases in equilibrium together in such systems to 3 ($\mathcal{F} = 0$) and if there are three phases in equilibrium they must do so at a fixed temperature and pressure (*i.e.*, the triple point). If a magnetic field is present in a unary system, the Gibbs Equilibrium Phase Rule becomes

$$\Phi + \mathcal{F} = 4$$

because of the additional intensive thermodynamic variable, \mathcal{H} . This is valid even if no magnetic phase is present, because all materials respond to the application of the magnetic field through their magnetic susceptibility.

In this paper, various examples of phase diagrams of materials which include paramagnetic-to-ferromagnetic *transitions* will be discussed. Such transformations are usually not *first-order transformations*, and therefore the common Gibbs Equilibrium Phase Rule does not always apply at surfaces or curves which delineate these non-first-order transformations. This is a result of the fact that equilibrium between the magnetically ordered and disordered phases does not obtain at their transition boundaries. Hence, the paramagnetic-to-ferromagnetic transformation is unlike the familiar first-order transformations usually studied in materials systems.

II. THE PARAMAGNETIC-TO-FERROMAGNETIC TRANSFORMATION

If paramagnetic-to-ferromagnetic transformations are to be included in equilibrium phase diagrams, the two states must be designated as different thermodynamic phases. This has not always been accepted by some metallurgists.^[2,3] Indeed the transformation in iron alloys of the ferromagnetic α phase to the paramagnetic BCC phase sometimes has not been considered to be a phase

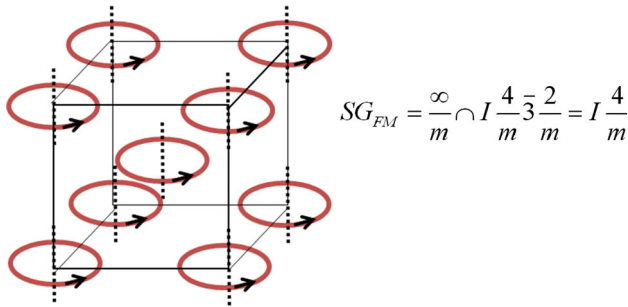


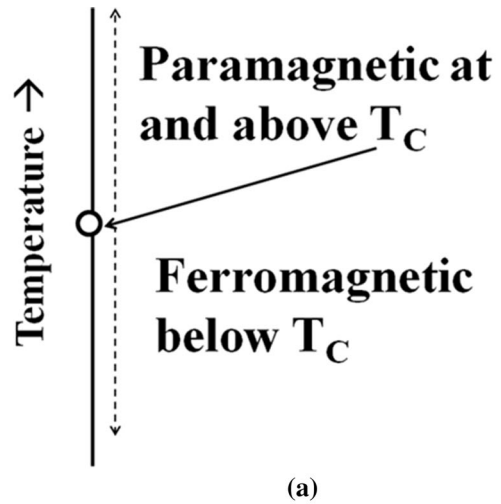
Fig. 1—Schematic of the crystal structure of ferromagnetic α iron. The circles with a direction of rotation represent the magnetic moments (spins) associated with each atom. It can be seen that the structure of the ferromagnetic iron is body-centered tetragonal ($I\frac{4}{m}$), since the vertical direction [001] is not equivalent to the directions [100] and [010]. Also mirror planes parallel to the uniaxial direction are not present. If the magnetic moments (spins) were randomly arrayed, the iron would display cubic symmetry ($Im\bar{3}m$). As shown in the figure, the space group of the ferromagnetic phase can be obtained by intersecting the symmetry of the axial magnetic moment vector with that of the paramagnetic space group.

transformation! See Reference 4 for a brief history of this discussion. However, the paramagnetic phase and the ferromagnetic phase not only have distinct magnetic properties but they also have distinct crystallographic symmetries. See Figure 1. This figure shows that the ferromagnetic α phase with a directional orientation of the magnetic moments (spins) on its atoms along its [001] direction has a uniaxial symmetry, not a cubic symmetry. On the other hand, the paramagnetic phase with random orientation of the moments does have the cubic BCC symmetry. Paramagnetic and ferromagnetic phases are distinct and have different regions of stability and therefore must be taken into account in phase diagrams of alloys which have equilibrium phases that are magnetic, be they ferromagnetic, antiferromagnetic, or ferromagnetic. In this paper, only the paramagnetic-to-ferromagnetic transformations will be discussed.

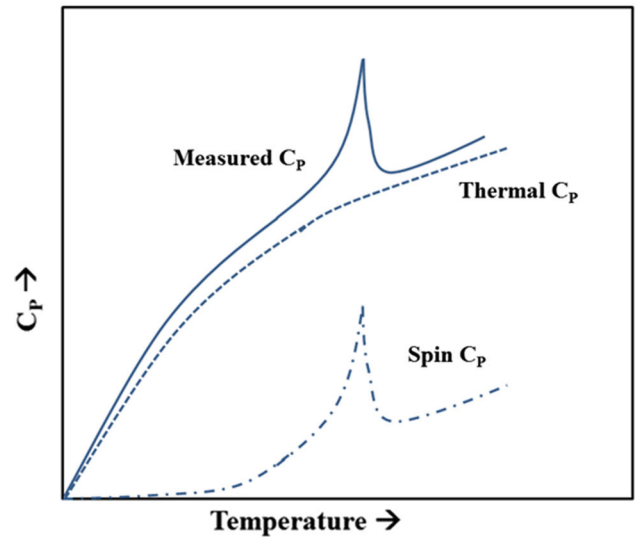
The paramagnetic-to-ferromagnetic transformation has been studied for well over a century. It is a prime example of a symmetry breaking transition in which a continuous symmetry of the magnetic moments (spins) in the paramagnetic phase reduces to a lower symmetry. In the case of Fe, the randomly oriented magnetic moments of the paramagnetic phase, with magnetic symmetry ∞m (or $O(3)$), are reduced to the uniaxial symmetry $\frac{\infty}{m}$, the symmetry of an axial vector which represents the magnetization. When the axial symmetry is aligned along the [001] and is intersected with the symmetry of a BCC structure, one obtains the space group for the ferromagnetic phase as $I\frac{4}{m}$. See Figure 1.* The spontaneous breaking of symmetry

*In this paper, I am not using the full magnetic symmetry group notation. For discussions of magnetic symmetry, see References 5 through 12

brings with it an order parameter (in this case, the magnetization, M), an emerging stable-ordered phase, ground-state excitations called magnons, as well as



(a)



(b)

Fig. 2—(a) A one-dimensional phase diagram of a magnetic material displaying regions of stability of the paramagnetic phase and the ferromagnetic phase as a function of temperature. At the Curie temperature (T_C), the stable phase is the paramagnetic phase. In this diagram, the pressure is constant and the applied magnetic field \mathcal{H} , is zero. (b). Schematic heat capacity plots of a magnetic material (solid curve) and its heat capacity due only to thermal effects (dotted curve). The difference between the two is shown as the spin heat capacity (dot-dash curve). The pressure is constant and there is no applied magnetic field.

defects such as magnetic domain walls and in some cases magnetic vortices.

III. THE CURIE TEMPERATURE

The transformation of a paramagnetic to ferromagnetic phase on cooling, begins immediately below a temperature called the Curie temperature (named after Pierre Curie, 1859–1906). Below the Curie temperature, the equilibrium phase has a different symmetry and a non-zero-order parameter, the magnetization M . At the Curie temperature, the phase present has a zero

magnetization and is therefore best described as the *paramagnetic* phase. See Figure 2(a).

The Curie temperature differs from temperatures which denote an invariant first-order transition such as the liquid-to-crystalline transformation of a pure component, in that the two phases (paramagnetic and ferromagnetic) do not coexist in equilibrium with each other at the Curie temperature. A schematic of the heat capacity *vs* temperature plot for a material undergoing a ferromagnetic-to-paramagnetic transformation is shown in Figure 2(b). As the temperature of the alloy approaches the Curie temperature from below, there is an anomalous increase in the heat capacity over and above the increase due to the increase in the thermal heat capacity: that is, over and above that which the heat capacity of the material would display if there were no magnetic transformation. See the dotted curve in the figure. Keesom and Keesom^[13] attribute Ehrenfest as the first to call such transitions Lambda Transitions because the heat capacity curve has the shape of the Greek letter *lambda*. Such transformations occur *continuously* in distinction with the abrupt first-order thermodynamic phase transformations. No latent heat is associated with Lambda Transitions at their transition temperature. This is the case for a large variety of order–disorder transformations. Lambda Transitions are not second-order transformations after the designation of Ehrenfest^[14]; they differ from a second-order transformation in their near divergence of the heat capacity as the temperature approaches T_C from below. See Pippard^[15] for a thorough discussion of these non-first-order transitions. These transitions are also called continuous or higher-order transformations. Since these magnetic transitions are not first order, the rules for the construction of the phase diagrams derived from the Gibbs Equilibrium Phase Rule need not apply. Examples are explored below.

IV. UNARY PHASE DIAGRAMS

We now discuss two-dimensional phase diagrams of one-component (unary) systems that contain a magnetic phase. In most thermodynamics texts, the phase diagrams of unary systems are those where the thermodynamic variables are temperature, pressure, or volume. In such a case, the molar Gibbs free energy (G) is introduced. For a single-component system, the molar Gibbs free energy is written as follows:

$$G \equiv H - TS = U + PV_m - TS, \quad [3]$$

$$dG = V_m dP - S dT, \quad [4]$$

where H is the molar enthalpy, T is the temperature, S is the molar entropy, P is the pressure, and V_m is the molar volume of the system. Equation [4] is obtained from Eq. [3] by using the combined First and Second Laws of Thermodynamics:

$$dU = TdS - PdV_m.$$

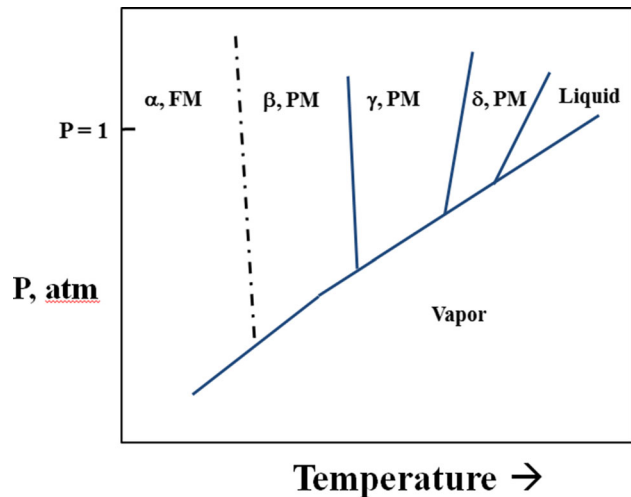


Fig. 3—Schematic of the pressure *vs* temperature plot of Fe with zero applied magnetic field. The magnetic transformation curve (Curie temperature as a function of pressure) is shown as a dot-dash curve to differentiate it from the first-order two-phase curves.

The phase(s) present in equilibrium is (are) the one(s) which have the minimum value of the Gibbs energy. Plots of pressure *vs* volume, pressure *vs* temperature, and volume *vs* temperature of simple one-component systems are often displayed in thermodynamic texts.

A schematic pressure–temperature phase diagram of Fe is shown in Figure 3. It can be seen that at low temperature and pressure $P = 1$ atm, the phase present is the ferromagnetic α phase. Upon heating at constant pressure, the α phase transforms into the paramagnetic BCC phase (β) at the dot-dash curve. The line is displayed as *dot-dash* to point out that there are not two phases in equilibrium along the curve; only the paramagnetic phase is present along the line, as discussed above.

The remaining solid-state phase changes which occur on heating, the β -to- γ and of γ -to- δ transitions are classical first-order phase changes. This distinction between first-order phase change and non-first-order phase change is important as the concomitant property changes during the transformations differ greatly. For example, the point of intersection of the dot-dash curve with the vapor curve is not a triple point because only two phases are in equilibrium at that point of the diagram, namely, the paramagnetic BCC Fe and the vapor phase of Fe. The points of intersection of the solid curves delineating equilibrium between the β and γ phases and the γ and δ phases with the vapor curve are triple points. So too is the intersection of the δ/L curve and the vapor curve. The solid lines of the diagram follow the Clapeyron equation for first-order transformations, namely,

$$\frac{dP}{dT} = \frac{\Delta S}{\Delta V}. \quad [5]$$

For the β/γ curve, $\Delta S > 0$ and $\Delta V < 0$, so the slope of the curve is negative. For the γ/δ curve, ΔS and ΔV are both positive so the slope of the curve is positive.

The slope of the Curie temperature curve cannot be determined by the Clapeyron equation since both, ΔS and ΔV , are equal to zero at the transition. Since, $\Delta S = 0$, we can set its total derivative, $d\Delta S$, equal to zero and obtain

$$\frac{dP}{dT} = \frac{\Delta C_P}{TV_m \Delta \alpha}, \quad [6]$$

where $\Delta \alpha$ is the change in the volume expansivity at the transition and ΔC_P is the change in the heat capacity at the transition temperature. The slope of $\frac{dP}{dT}$ for the α -to- β transition in iron is very large so the Curie curve is nearly vertical.

V. THERMODYNAMICS OF UNARY SYSTEMS WITH MAGNETIC PHASES

In considering the thermodynamics of alloy systems that contain magnetic phases, we must include the intensive variable of the applied magnetic field, \mathcal{H} and its conjugate extensive variable of magnetization, \mathbf{M} .

The combined First and Second Laws of Thermodynamics is now written to include the magnetic work term

$$dU = TdS - PdV + \mu_0 V_m \mathcal{H} d\mathbf{M}, \quad [7]$$

where μ_0 is the permeability of vacuum. As can be seen from the equation, applying a magnetic field displaces (aligns) the magnetic moments and hence work is done on the system, thereby increasing its internal energy.

By Legendre transforms, Gibbs free energy-type thermodynamic potentials can be written in differential form either as^[16]

$$dG = -SdT + VdP + \mu_0 V_m \mathcal{H} d\mathbf{M} \quad [8a]$$

or as

$$dG = -SdT + VdP - \mu_0 V_m \mathbf{M} d\mathcal{H}. \quad [8b]$$

Equation [8a] gives $G = G(T, P, \mathbf{M})$, in which the Gibbs free energy is a function of the independent intensive variables, T and P , as well as the extensive variable of the magnetization, \mathbf{M} .

At constant P ,

$$dG = -SdT + \mu_0 V_m \mathcal{H} d\mathbf{M}. \quad [9]$$

Therefore $G = G(T, \mathbf{M})$. We now follow the approach introduced by Landau and Lifshitz^[5] and expand the free energy as a Taylor series function of the magnetization about the transition temperature, T_C .

$$G = G_0 + a(T - T_C)\mathbf{M}^2 + b\mathbf{M}^4. \quad [10]$$

Here, a and b are positive constants and only even values of the power of \mathbf{M} are included because of the symmetry of the magnetized state. The temperature T_C

is the Curie temperature, at and above which the system is disordered ($\mathbf{M} = 0$).

For equilibrium, G must be a minimum, thus we have

$$\left(\frac{\partial G}{\partial \mathbf{M}}\right)_T = 0 = 2a(T - T_C)\mathbf{M} + 4b\mathbf{M}^3. \quad [11]$$

The roots of this equation are

$$\mathbf{M} = 0 \quad \text{and} \quad \mathbf{M}^2 = -\frac{a(T - T_C)}{2b}. \quad [12]$$

For $T \geq T_C$, $\mathbf{M} = 0$, which is the paramagnetic phase (disordered, high symmetry).

For $T < T_C$, \mathbf{M} is non-zero, which is the ferromagnetic phase (ordered, lower symmetry). The transition temperature can be found by setting \mathbf{M} equal to unity at $T = 0$ and is

$$T_C = \frac{2b}{a}.$$

Figure 4 shows plots of G vs \mathbf{M} and \mathcal{H} vs \mathbf{M} for temperatures above (a and b) and below (c, d) the Curie temperature.

Figure 4(a) shows that at temperatures above the Curie temperature, any fluctuation which increases the magnetization also increases the free energy; hence the fluctuation in order parameter will diminish. (That is the meaning of a minimum in free energy being the equilibrium state!). Figure 4(b) plots the intensive variable of the magnetic field, $\mathcal{H} = \left(\frac{\partial G}{\partial \mathbf{M}}\right)_{P,T}$ vs magnetization displaying the \mathcal{H} - \mathbf{M} phase diagram of a paramagnetic material. At large fields, the magnetization reaches a maximum (saturation). When the field is reversed, the value of \mathbf{M} passes through zero, with a non-zero but finite slope, $\frac{1}{\chi} = \left(\frac{\partial \mathcal{H}}{\partial \mathbf{M}}\right)_{P,T}$, on its way to saturating in the opposite direction. (Here, χ is the magnetic susceptibility.)

Figure 4(c) displays the plot of G vs \mathbf{M} at a temperature below the Curie temperature. Here, G is a maximum at $\mathbf{M} = 0$, indicating that the paramagnetic phase ($\mathbf{M} = 0$) is unstable. In this model, there are two equilibrium states with equal and opposite values of \mathbf{M} . If the system is cooled very slowly with no applied magnetic field, the system transforms to either or both of the two states (Y or X, see Figure 4(d)). This process is known as *spontaneous symmetry breaking*. If, however, a magnetic field is applied to the system during cooling, a term must be added to Eq. [10] which favors the formation of one of the states. This kind of transformation, occurring under an applied magnetic field, is known as one with an *explicit breaking of symmetry*, since the equilibrium state (X or Y) is determined by the direction of the magnetic field. Figure 4(d) plots the intensive variable of the magnetic field, $\mathcal{H} = \left(\frac{\partial G}{\partial \mathbf{M}}\right)_{P,T}$ vs magnetization and displays the \mathcal{H} - \mathbf{M} phase diagram of a ferromagnetic material. At large magnetic fields, the magnetization reaches a maximum and when the field is reversed the value of

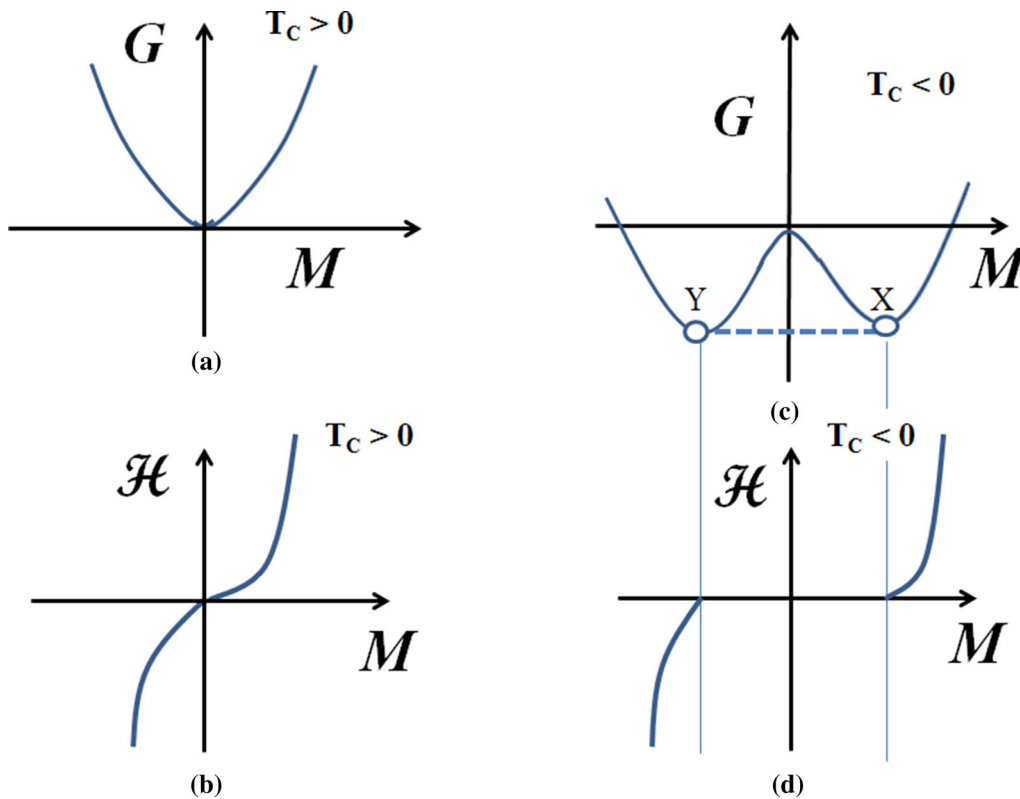


Fig. 4—The Gibbs free energy vs M plots and the \mathcal{H} vs M plots for $T > T_C$ (a and b) and for $T < T_C$ (c and d). Below T_C , one of the two possible states with non-zero M (X or Y) is stable even when $\mathcal{H} = 0$. The pressure is assumed to be constant in these plots.

M changes discontinuously at zero field to the negative value of the magnetization.

The equilibrium phase diagrams of M vs T and \mathcal{H} vs T are shown in Figures 5(a) and (b). At and above T_C , the phase in equilibrium is the paramagnetic phase, while below T_C the phase present is the ferromagnetic phase. In Figure 5(a), the two possible states present below T_C are delineated as X and Y. Compare with Figure 4(c). If a large enough magnetic field is applied in the downward direction to the system in state X, it will change the system to one in state Y. See also Figure 4(d). This change of state is *discontinuous* since there is an energy barrier to overcome.

Figure 5(b) shows that at zero applied field, the possible states are either paramagnetic or ferromagnetic, depending on the temperature. The slope of the \mathcal{H} vs T curve is zero, since for a discontinuous change from state X to state Y the slope $(\frac{\partial \mathcal{H}}{\partial T})_P$, is proportional to the change in entropy in going between the two states, which in this case is zero, since both states X and Y have the same degree of magnetic order.

In the phase diagram displayed in Figure 3, the thermodynamic variables are the intensive ones of pressure and temperature. If we allow for the application of an external magnetic field, an extra degree of freedom must be accounted for. The phase diagram would be a three-dimensional P - T - \mathcal{H} diagram.

The effect of a non-zero applied magnetic field on the first-order lines of this pressure temperature diagram is shown in Figure 6. This is a section through P - T - \mathcal{H}

space at a fixed field, \mathcal{H} . The application of \mathcal{H} causes a shift in the two-phase equilibrium curves from their positions in the $\mathcal{H} = 0$ plot (Figure 3). It can be seen that the β/γ coexistence curve is shifted to higher temperatures and the γ/δ curve is shifted to lower temperatures. This occurs since the magnetic susceptibilities (χ) of β and δ are greater than that of γ at their transformation temperatures. In both cases, the phase with the greater magnetic susceptibility has its region of stability increased.

This shifting of the two-phase equilibrium curves follows from the thermodynamic expression for the Gibbs free energy in Eq. [8b]

$$dG = -SdT + VdP - \mu_0 V_m M d\mathcal{H}. \quad [13]$$

In the linear region of the M - \mathcal{H} curve, we have

$$\chi \equiv \frac{M}{\mathcal{H}}. \quad [14]$$

Thus at constant pressure and temperature, we write for each phase

$$dG_i = -\mu_0 V_m^i \chi_i \mathcal{H} d\mathcal{H}. \quad [15]$$

It can be seen that increasing the magnetic field lowers the Gibbs energy to a greater extent for the phase which has the larger magnetic susceptibility. Thus, increasing the external magnetic field increases the regions of

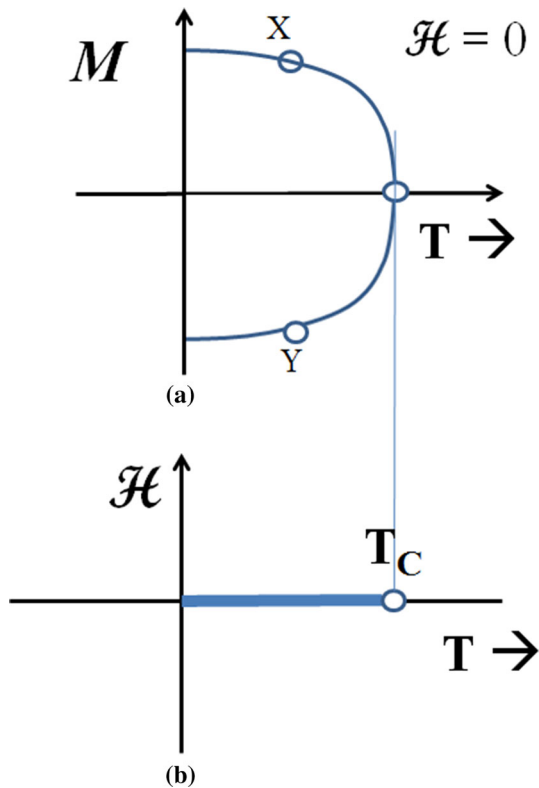


Fig. 5—(a) The order parameter M , vs T plot for the two possible magnetic states (domains). State X can be changed to state Y discontinuously by the application of a suitably oriented magnetic field. (b) Magnetic field \mathcal{H} vs T plot showing that the transition occurs at T_C without the application of a magnetic field. In both diagrams, the pressure is held constant.

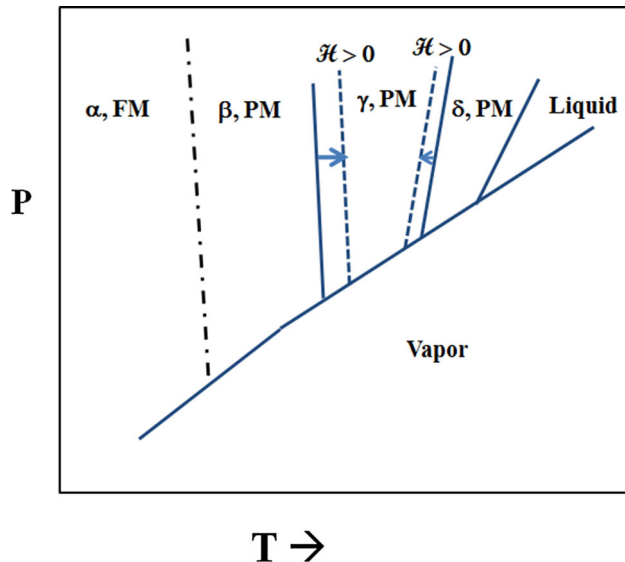


Fig. 6—Schematic of the pressure vs temperature plot of Fe with zero applied magnetic field (solid coexistence curves) and an applied external magnetic field \mathcal{H} (dashed coexistence curves). The application of the field shifts the coexistence curves in the direction which increases the stability region of the phase with the larger magnetic susceptibility, χ .

stability of the phases with largest magnetic susceptibilities. At very large applied magnetic fields, the FCC γ phase would be absent at ambient pressure.

In this diagram, the Curie temperature curve would shift to the higher temperature with the application of a magnetic field since the field stabilizes the magnetic phase, but this is not displayed in the figure.

VI. PHASE DIAGRAMS OF BINARY ALLOYS: NO APPLIED MAGNETIC FIELD H

A. Case 1: Curie Temperature Curves that Do Not Intersect Other Phase Boundaries

When we investigate the temperature composition phase diagrams of a binary system of a ferromagnetic element A with the element B, a question naturally arises: how will the Curie temperature vary with the addition of the second element? As with most such questions, the answer depends on the intrinsic properties of the elements A and B. For example, if Ni is added to Co we expect the Curie temperature of the Co-rich alloy to decrease, since the Curie temperature of Ni is less than that of Co. This can be rationalized from the Hamiltonian of the Co-Ni alloy (written in terms of the Heisenberg exchange), since on average the *exchange energy* of such an alloy decreases because of the addition of the second element with a lower Curie temperature. A phase diagram of Co-Ni is shown in Figure 7. This equilibrium phase diagram displays the Curie temperature of the FCC solid solution of Co and Ni as a function of composition. On the diagram, the Curie temperature as a function of composition is designated by a dot-dash curve. At and above the Curie temperature, the alloy is FCC and paramagnetic. Below the Curie temperature, the alloy is ferromagnetic and has rhombohedral symmetry because the magnetic moments of the ferromagnetic phase are aligned along one of the former $\langle 111 \rangle$ directions of the FCC paramagnetic phase.

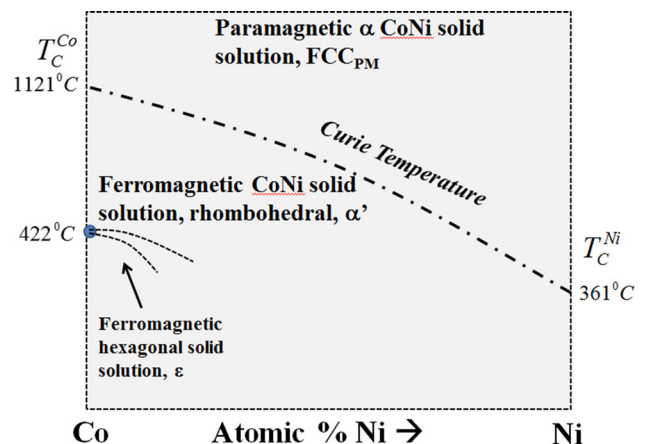


Fig. 7—The Co-Ni binary-phase diagram. The Curie temperature is denoted by the dot-dash line. The Co-rich alloys displays a structural transition to a ferromagnetic hexagonal phase below 422°C . The curves represent first-order phase boundaries, but are dashed because they are not accurately known. The pressure is atmospheric and there is no applied magnetic field.

The Co-rich side of the diagram has some features which need explanation. It can be seen that below 422 °C, Co is designated as the ϵ phase, which is a ferromagnetic version of HCP. Its space group is $P6_3/m$, since the magnetic moments are aligned along the [0001] of the ϵ phase. Above this temperature, pure ferromagnetic Co has rhombohedral-distorted FCC symmetry. In Co, the transformation of the ferromagnetic ϵ phase to the ferromagnetic α phase Co phase is not a magnetic transformation: it is a structural transformation. The change in the stacking sequence of the close packed planes for this transformation causes the transformation to be sluggish (a reconstructive type). It also necessitates it be a thermodynamically first-order transformation. At 422 °C, both the ferromagnetic phases of pure Co may coexist in equilibrium.

Below 422 °C, as Ni is added to Co, the temperature of the structural transformation temperature is lowered, and a two-phase region opens up in which two ferromagnetic phases coexist: one is the hexagonal ϵ phase, and the other is the rhombohedral α' phase. The curves are dashed because they are not known with precision, because of the sluggishness of the transformation between the hexagonal and rhombohedral ferromagnetic phases. The curves are first order phase boundaries.

Figure 8 is a schematic of the diagram drawn to 0 K, assuming that the ground state of the alloy consists of two ferromagnetic phases: one ferromagnetic Co (ϵ_{FM}) and the other ferromagnetic Ni (α'_{FM}). Such a diagram is in conformity with the restraints of the Third Law of Thermodynamics since at 0 K, the two phases present have no configurational entropy (they are the elements Co and Ni) and no magnetic spin entropy since they are fully ordered magnetically.^[17,18] The horizontal lines in the two-phase field are tie lines. The space groups of the phases at 0 K are $P6_3/m$ and $R\bar{3}$ for the Co and Ni phases, respectively.

B. Case 2: Curie Temperature Curves that Intersect First-Order Phase Boundaries

1. The Fe-C phase diagram

The Fe-C binary diagram is one of the most studied and discussed diagrams in the metallurgical literature. It contains the transformation of the BCC paramagnetic (β) phase to the low-temperature ferromagnetic α phase.**

**The rationale for returning to the designation of the paramagnetic BCC phase of Fe as the β phase is discussed in References 4 and 18.

An exaggerated schematic of the diagram in the Fe-rich region as it often appeared in the early 20th century is shown in Figure 9. The addition of C to Fe lowers the Curie temperature of the alloy (very slightly) and the Curie curve is seen to intersect with a two-phase region consisting of the γ , FCC paramagnetic phase, and the BCC-based phases, α and β . In the figure, the intersection is denoted by a dot: this represents the Curie temperature of the ferromagnetic α phase of Fe which is saturated

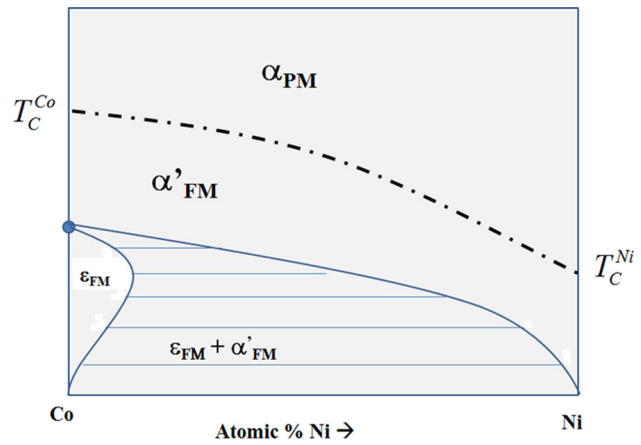


Fig. 8—A schematic of the Co-Ni binary-phase diagram which shows how the lower region of the diagram may look in keeping with the Third Law of Thermodynamics. Other configurations are possible if, for example, an intermetallic phase exists in the Co-Ni system.

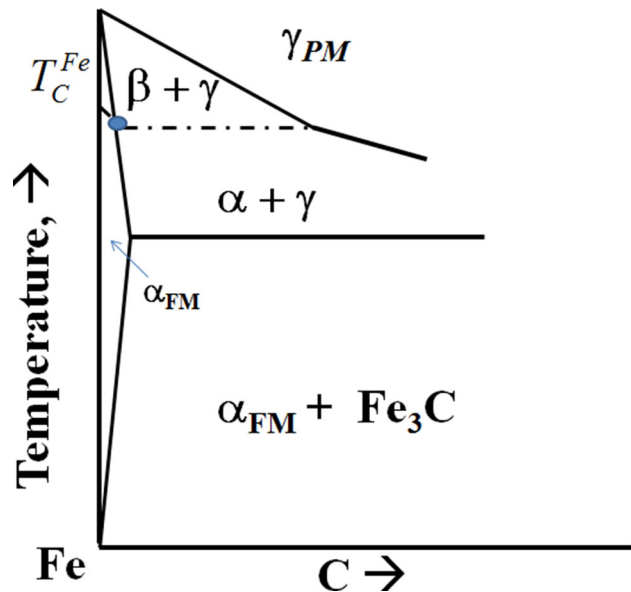


Fig. 9—Schematic of a portion of the metastable Fe-C phase diagram as depicted in the early 20th century. The intersection of the Curie line with the two-phase field produces 2 two-phase regions separated by a horizontal line (*dot-dash*) which denotes the Curie temperature of the α_{FM} phase which is saturated with C.

with C at that temperature. All alloys within the two-phase region will on heating have their α , ferromagnetic phase transform to the paramagnetic β phase at the temperature shown by the horizontal dot-dash line. This horizontal line does not denote three-phase equilibrium: rather, it demarks the Curie temperature of the α phase of alloys with their compositions within the region. At and above the dot-dash line, the phases present are paramagnetic γ phase and paramagnetic BCC β phase. Below the dot-dash line, the phases present are ferromagnetic α phase and the FCC paramagnetic γ phase. Both of these regions are two-phase regions but they are not separated

by a three-phase invariant temperature line as is the case for first-order phase transformations.

Figure 9 portrays an interesting feature that often appeared in early 20th-century Fe-C-phase diagrams, which is a change in the slope of the γ /ferrite transformation curve at its intersection with the horizontal Curie line. This is in keeping with the fact that the phases in equilibrium with the γ phase are different above and below the Curie temperature. This means that their free energies would be different and that the common tangent of their respective free energy plots would differ slightly. The change in slope would be very small. An example of a phase diagram showing this change in slope is Figure A of McCance's correspondence on the Hondo and Takaki paper.^[2] Modern phase diagrams do not show this change in slope.

2. Intersection of Curie temperature curve with a miscibility gap

More than 50 years ago, Meijering^[19] published a paper in which he discussed various effects that occur when the Curie temperature curve of a ferromagnetic transformation intersects a miscibility gap in a binary-phase diagram. Figure 10 is adopted from Figures 1 and 2 of his paper. It can be seen that when the Curie curve intersects the miscibility gap, an indentation appears in the phase boundary of the miscibility gap (exaggerated in the figure). This occurs because at the point of intersection, the free energy curve of the ferromagnetic phase departs from that of the double-hump free energy curve of the disordered phases of the miscibility gap. The common tangent construction produces a phase with a slightly less solubility of B in the ferromagnetic phase than in the paramagnetic phase at the temperature of the intersection (T_1). The gap is now divided into two regions: one with the α'_{PM} and α''_{PM} phases and the other with the α'_{FM} and α''_{PM} phases present. See Figure 10(b). The former is a miscibility gap but the latter is a two-phase region consisting of a paramagnetic phase and a ferromag-

[†]The region with the two phases α'_{FM} and α''_{PM} is not a miscibility gap because it is made up of two phases with different crystal symmetries. This means that their free energy curves are distinct from one another. See Figure 10(a).

netic phase.[†] The horizontal line between these two-phase regions is the Curie temperature of the ferromagnetic phase which forms at the intersection with the miscibility gap. An alloy which has the critical composition (X_c) first decomposes into two paramagnetic phases on cooling. The regions enriched in A transform continuously into a ferromagnetic phase at the temperature T_1 , denoted by the horizontal *dot-dash* line. As in the case of the Fe-C diagram, the horizontal line is not a three-phase invariant line: rather it denotes the Curie temperature of the alloys within the two phase $\alpha'_{PM}/\alpha''_{PM}$ region.

Figure 10(a) shows that the free energy of the ferromagnetic phase departs from the paramagnetic free energy curve smoothly as is expected for a higher-order

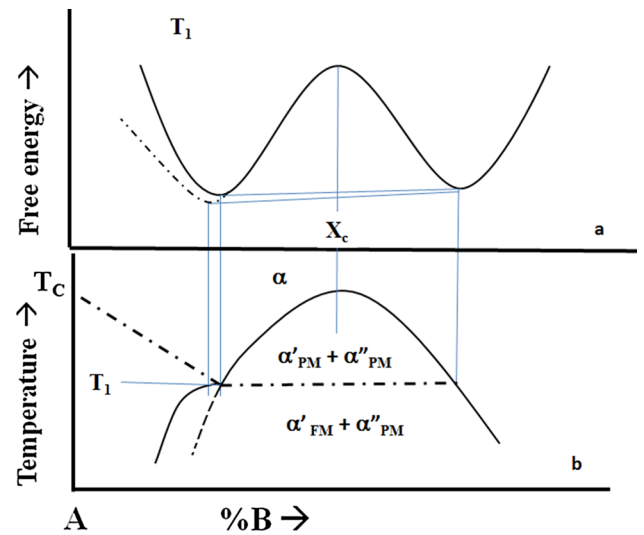


Fig. 10—Schematic phase diagram showing the intersection of the Curie temperature curve with a miscibility gap. The intersection causes a slight change in the solubility of the B solute in the ferromagnetic material. The horizontal line is the Curie temperature of all alloys which lie within the two-phase $\alpha'_{PM}/\alpha''_{PM}$ phase field. The *dot-dash* line is the Curie curve and the dashed line is the metastable continuation of the miscibility gap of the two paramagnetic phases (after Meijering^[19]).

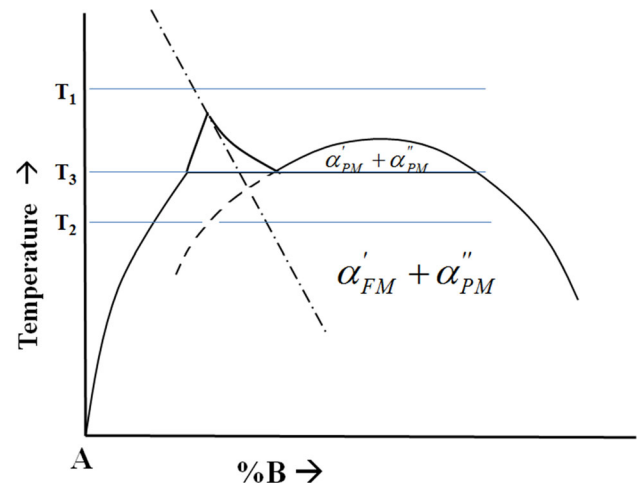


Fig. 11—Schematic of the intersection of the Curie temperature curve causing a horn-like two-phase region. The horizontal line is an invariant three-phase region displaying a monotectoid-like topology. Free energy curves for the three temperatures are shown in Figs. 12, 13, and 15. The dashed line is the metastable continuation of the miscibility gap of the two paramagnetic phase. In the diagram, the pressure is constant and the applied magnetic field is zero.

transition. The two common tangents drawn from the solute-rich minimum to the solute-lean minima display the slight differences in solubility that exists in the phases above and below the horizontal line. The indentation on the B-rich side of the gap is smaller and is not depicted in the figure.

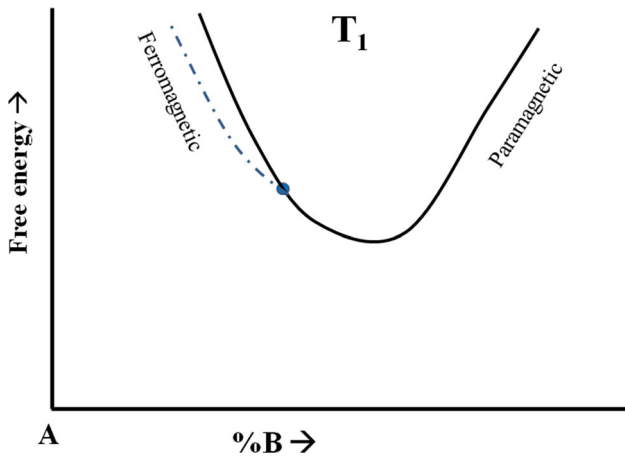


Fig. 12—Schematic of the free energy curve at T_1 of the alloy system of Fig. 11. The dot designates the composition of the phase which has T_1 as its Curie temperature.

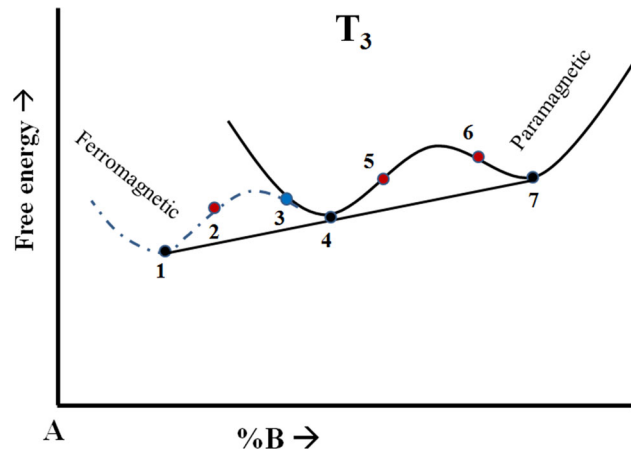


Fig. 13—Schematic of the free energy curves at T_3 of the alloy system of Fig. 11. The dots 1, 4, and 7 represent the compositions of the three phases in equilibrium at this temperature. Dots 2 and 3 are spinodals of the ferromagnetic phase and dots 5 and 6 are spinodals of the paramagnetic phase.

3. Curie temperature curve inducing a stable tricritical point

Another phase diagram that Meijering presented in his 1963 paper^[19] is shown in Figure 11. In this case, the intersection of the Curie temperature curve is closer to the critical point of the miscibility gap and the ferromagnetic phase displays a metastable gap. The horn-like two-phase region is a particularly interesting feature of this diagram. Note that an invariant three-phase line appears at T_3 , which resembles that of a monotectoid. This invariant line shows the coexistence of two paramagnetic phases and a ferromagnetic phase. Below the horizontal line, the equilibrium two-phase region consists of a ferromagnetic phase and paramagnetic phase.

The intersection of the Curie curve with the ordered spinodal curve has been termed a *tricritical point*. Sometimes, the tricritical point is a metastable one (that is, the intersection is within the two-phase portion shaped like a horn).^[20] If the tip of the horn is the point of intersection, the tricritical point is a stable one. This is the type we will discuss in this section. See References 21 through 24 for further discussion of this type of phase diagram.

Figure 12 displays a free energy plot for the alloy system depicted in Figure 11 at temperature T_1 . The branch of the curve representing the ferromagnetic phase (α_{FM}) leaves the free energy curve of the paramagnetic phase (α_{PM}) continuously, displaying the *higher-order character* of the formation of a ferromagnetic phase from a paramagnetic phase. Paramagnetic alloys with compositions of B less than that represented by the dot are unstable with respect to magnetic ordering. At temperature T_3 (Figure 13), three-phase equilibria is displayed and this is denoted by a triple tangent line connecting the ferromagnetic phase with the two paramagnetic phases. The composition of each of the phases in equilibrium is denoted by the three dots (1, 4, and 7). This figure shows that both the ferromagnetic phase and the paramagnetic phase display miscibility gaps. Point 2 is a spinodal of the ferromagnetic phase and point 3 is

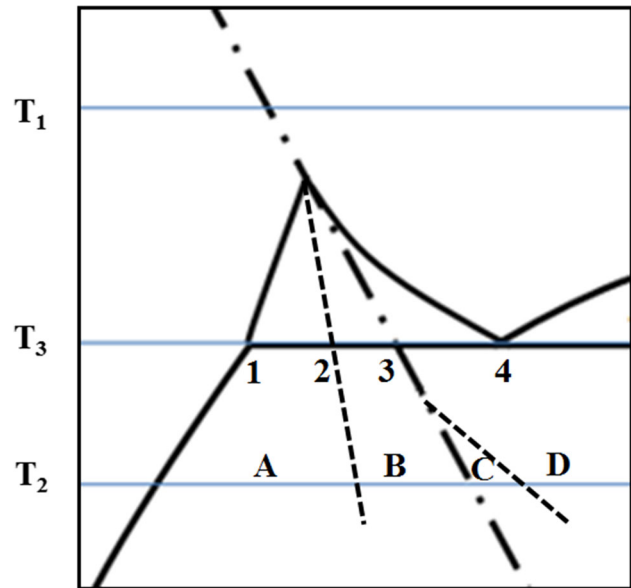


Fig. 14—A portion of the phase diagram displayed in Fig. 11, including lines of phase instability. The dot-dash curve is the Curie curve and a spinodal curve for the ferromagnetic phase. The dashed curves are the spinodal curves for the ferromagnetic phase and the paramagnetic phase (left to right). The Curie curve corresponds to the higher solute spinodal curve of the ferromagnetic phase.

the Curie curve composition at this temperature which coincides with the other spinodal of the ferromagnetic phase. The dots 5 and 6 are the spinodals of the paramagnetic phase at T_3 .

Figure 14 shows an enlarged portion of the phase diagram in the region of interest, and the dots denoted as 1, 2, 3, and 4 are those denoted in the free energy plot of Figure 13. Figure 14 includes the solute-lean spinodal curve of the ferromagnetic alloy which is not depicted in Figure 11.

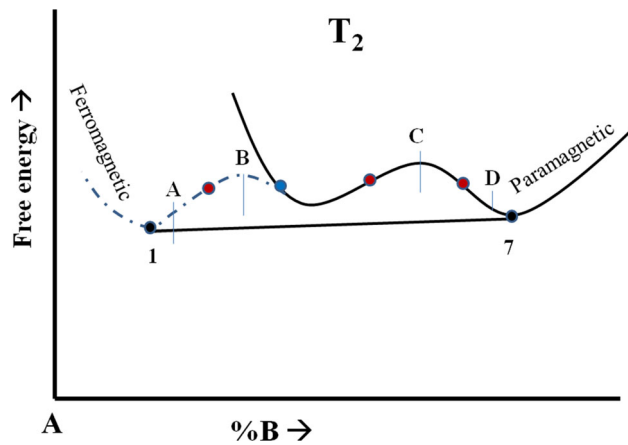


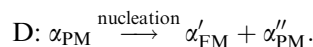
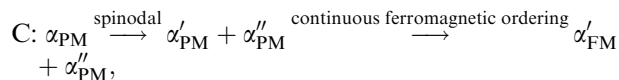
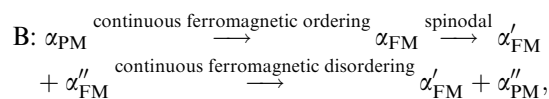
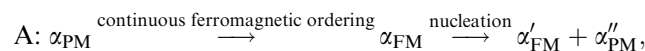
Fig. 15—Free energy plots of the ferromagnetic and paramagnetic phases at temperature T_2 . Both phases have miscibility gaps. The dots 1 and 7 represent the compositions of the equilibrium phases. The other dots are the spinodals for the respective phases.

Figure 15 is the free energy plot at T_2 , which shows the low-temperature two-phase equilibrium of the ferromagnetic phase and the paramagnetic phase as well as the location of the various phase instabilities. The regions denoted by the letters A, B, C, and D correspond to the regions with the same notation in the phase diagram of Figure 14.

From Figures 13 and 15, it can be seen that the Curie curve intersects the B-rich spinodal of the ferromagnetic phase at all temperatures. As indicated above, the tip of the horn is denoted as the *tricritical point*.

It is of interest to delineate the various transformation paths that occur in an alloy with this phase diagram configuration. In each case, the initial state is that of the high-symmetry phase (α_{PM}) and then the alloy is quenched to the temperature T_2 . See Figures 14 and 15.

Quenching alloys of compositions in the ranges denoted as A, B, C, and D result in the following transformation paths.



The final state for each of the transformation paths contains the ferromagnetic phase (α'_{FM}) and the paramagnetic phase (α''_{PM}). Of course the amount of each of the phases varies following the lever rule. Also, the microstructure features will vary from sample to sample

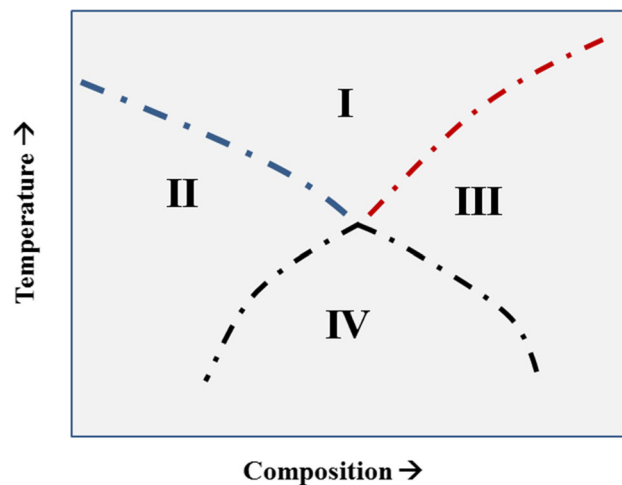


Fig. 16—A schematic of the phase diagram that Landau presented in Ref. [25]. The dot-dash curves represent higher-order transition curves. This represents a possible configuration of the higher-order transition curves around a tetracritical point. All phase regions are single phase. The pressure is constant and there is no applied magnetic field.

as well, since the instability transformations leave behind characteristic morphologies and boundaries within the final microstructure.

VII. PHASE DIAGRAMS WITH MULTIPLE HIGHER-ORDER TRANSITIONS

A. Tetracritical Points

Phase diagrams with intersecting Curie curves (or transitions of higher order) were first discussed by Landau in 1937.^[25] See also References 26 and 27. Landau's Figure 3 is redrawn and shown in Figure 16. He noted that the stable phase in region I is the high-symmetry phase, and that both the phases in regions II and III have symmetries which are subgroups of the symmetry of the phase in region I. Landau also noted that phase in region IV has a symmetry which is a subgroup of both phase II and III as well as a subgroup of the phase in region I.

The diagram is redrawn in Figure 17 to show possible ordered phases which would give rise to such an intersection. Extensions of the ordering transition curves into the single-phase region of the doubly ordered phase ($B2_{FM}$) are shown as thinner dot-dash curves. The phase with the most symmetry in the case shown in Figure 17 is the paramagnetic BCC phase ($A2_{PM}, Im\bar{3}m$). The ferromagnetic version of this phase ($A2_{FM}, I\frac{4}{m}$) and the atomically ordered version ($B2_{PM}, Pm\bar{3}m$) are both subgroups of the $A2_{PM}$ phase. Lastly, the ferromagnetic atomically ordered phase ($B2_{FM}, P\frac{4}{m}$) has a symmetry which is a subgroup of all three of the previous mentioned phases.

In the phase diagram shown in Figure 17, four critical curves are seen to meet at a point, called the *tetracritical point*. The four critical curves are as follows:

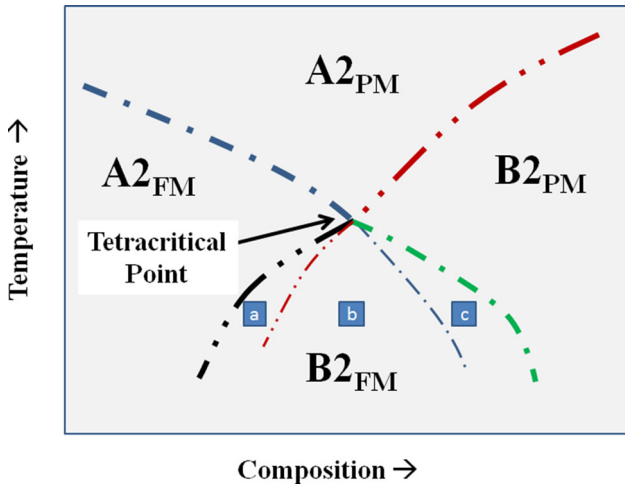


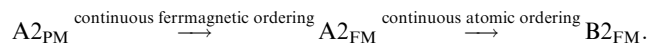
Fig. 17—This figure replots the tetracritical phase diagram of Fig. 16, and includes specific types of phases which could occupy the four single-phase regions around a tetracritical point. The dot-dash curves represent Curie curves, and the dot-dot-dash curves represent higher-order transition atomic ordering curves. The thinner curves are extrapolations of the high-temperature higher-order transition curves.

- Curie temperature curve for the A2 phase:
 $A2_{PM} \xrightarrow{\text{continuous ferrimagnetic ordering}} A2_{FM}$,
- Atomic disorder to order curve for the A2 phase:
 $A2_{PM} \xrightarrow{\text{continuous atomic ordering}} B2_{PM}$,
- Atomic disorder to order curve for the A2_{FM} phase:
 $A2_{FM} \xrightarrow{\text{continuous atomic ordering}} B2_{FM}$,
- Curie temperature curve for the B2_{PM} phase:
 $B2_{PM} \xrightarrow{\text{continuous ferrimagnetic ordering}} B2_{FM}$.

At the *tetracritical* point, the three ordered phases become disordered and the only phase present in equilibrium is the high-temperature, high-symmetry disordered A2_{PM} phase.

Again it is of interest to examine different transition paths that can occur in various alloys in such a phase diagram.

An alloy quenched from the A2_{PM} phase to region “a” in the diagram is unstable with respect to magnetic ordering and then the A2_{FM} phase is unstable with respect to atomic ordering. The transition is summarized as:



An alloy quenched to “b” lies below the extension of the A2 Curie temperature and would therefore become ferromagnetic before continuously ordering atomically from A2_{FM} to B2_{FM}.

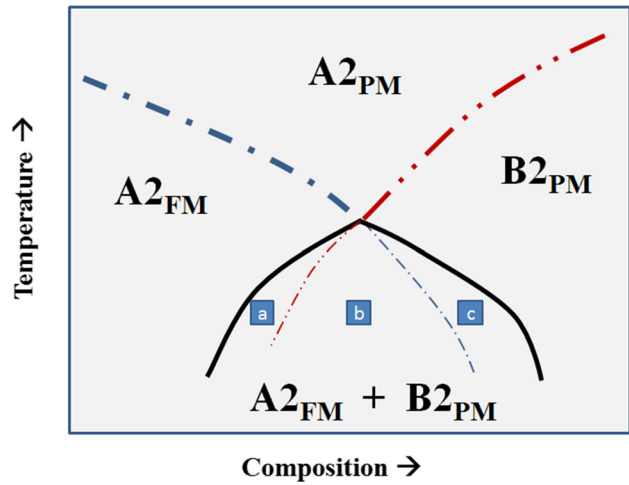
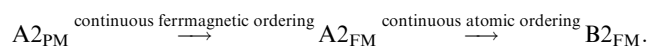
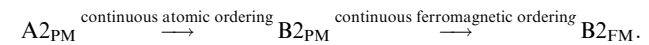


Fig. 18—A phase diagram of an alloy system exhibiting a bicritical point. The dot-dash curve represents the Curie curve of the A2 phase and the dot-dot-dash curve represents the higher-order atomic ordering transition curve for the A2 phase. The solid curves are the phase boundaries of the equilibrium two-phase region comprised of the A2_{FM} and B2_{PM} phases.

These two paths are identical because in both cases, the alloy is at a temperature below the magnetic transition A2_{PM} to A2_{FM} which must occur before the atomically ordered ferromagnetic B2 phase can form. Such a transition has been called a “contingent ordering transition” since its occurrence is contingent on the *prior* magnetic ordering.

An alloy quenched to “c,” however, is above the extension of the Curie curve for A2_{PM} to A2_{FM} and hence undergoes atomic ordering first (continuously) followed by the continuous ferromagnetic transition to the B2 ferromagnetic phase.



In this case, the ferromagnetic ordering transition is contingent on the prior atomic ordering transition of A2_{PM} to B2_{PM}.

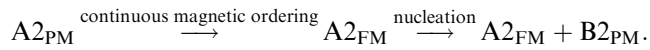
It should be noted that in all cases the final state is that of the B2_{FM} phase which as pointed out above has a symmetry which is a subgroup of each of the phases A2_{PM}, A2_{FM}, and B2_{PM}. However, the microstructures of the alloys in their final state would differ because of the various types of domains (magnetic domains and translational domains) as well as the specific locations of the domains which depend on the specific sequence of transformations. The FeSi binary alloy system may have such a tetracritical point in its phase diagram.^[28,29]

B. Bicritical point

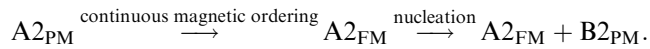
There is another interesting configuration that may occur when two higher-order transition curves intersect, namely, the *bicritical configuration*. A phase diagram with a *bicritical* point is displayed in Figure 18. For this type of intersection, the phase field directly below the

bicritical point is a two-phase field. In this case, the phase field boundaries are drawn solid since they represent first-order phase boundaries. This affects the way the high-temperature high-symmetry phase decomposes at lower temperatures.

An alloy quenched from the high-temperature A_{2PM} phase field to “a,” first magnetically orders to the A_{2FM} phase. The A_{2FM} phase is a supersaturated metastable phase until the stable B_{2PM} phase nucleates from it. The sequence is as follows:

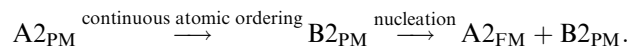


An alloy quenched from the high-temperature A_{2PM} phase field to “b” undergoes the following transition path:



This path is the same path as the previous one, since the instability curve for the atomic ordering transition is for paramagnetic phases: A_{2PM} to B_{2PM} . Once the A_{2PM} -to- A_{2FM} transition has occurred, the atomic ordering transition must occur by a nucleation and growth process.

An alloy quenched from the high-temperature A_{2PM} phase field to “c” undergoes the following transition path:



Here the atomic ordering process can occur continuously but the magnetic A_{2FM} phase must nucleate from it. Once again all three transitions end up with the same phases being present, namely, the A_{2FM} and the B_{2PM} phases. However, the transition paths and hence their microstructure differ.

The above descriptions of the transformation paths shown in Figures 14, 17, and 18 are thermodynamic in character. The proposed sequences are based on the assumption that unstable transitions occur before first-order transformations (nucleation). Also it is assumed that if the alloy is quenched below both instability curves, the higher-order magnetic transition occurs before the higher-order atomic ordering transitions because the magnetic transitions do not require atomic diffusion. The resulting microstructures can be quite complex as the various ordering transitions may give rise to translational and/or magnetic domains which will complicate the interpretation of the transitions if only observed by microscopy techniques. The resulting complex microstructures give rise to interesting magnetic and physical properties.

VIII. EFFECT OF APPLIED MAGNETIC FIELDS ON BINARY-PHASE DIAGRAMS

The common binary equilibrium phase diagrams which are utilized by materials scientists display equilibrium for systems whose independent variables are

composition and temperature with the pressure held constant. If a magnetic field is applied to a material, the system gains a degree of freedom and the phase diagram projected to the temperature composition plane changes. For example, in the Fe-C system, an applied magnetic field increases the eutectoid temperature because the stability field of the ferromagnetic α phase and the cementite phase increases with applied magnetic field. Similar to the ternary pseudobinary diagrams, this opens the three-phase invariant eutectoid line into a three-phase field and shifts the eutectoid composition to higher carbon compositions. The eutectoid transformation is no longer an invariant. See Figure 19.^[30]

Consider a binary Fe-C alloy at the eutectoid composition with no applied magnetic field. Three phases would be in equilibrium, namely, the α_{FM} , γ_{PM} , and Fe_3C phases. When an external magnetic field is applied, the α_{FM} -free energy decreases more than the other two free energy curves because its susceptibility is larger than that of the other phases. Thus, the three-phase equilibrium is disturbed, and the alloy moves into the two-phase α_{FM} plus Fe_3C phase field. The applied field increases the temperature of the three-phase eutectoid region. This implies that under the influence of a magnetic field, an alloy with composition greater than that of the binary eutectoid composition could decompose into a fully pearlitic constituent. When the temperature is lowered to room temperature and the magnetic field is removed, the microstructure would remain in this state unless it is heated. Joo *et al.*^[31] have some experimental data that are consistent with this effect. Much work is being done on this topic. See also References 32 through 34.

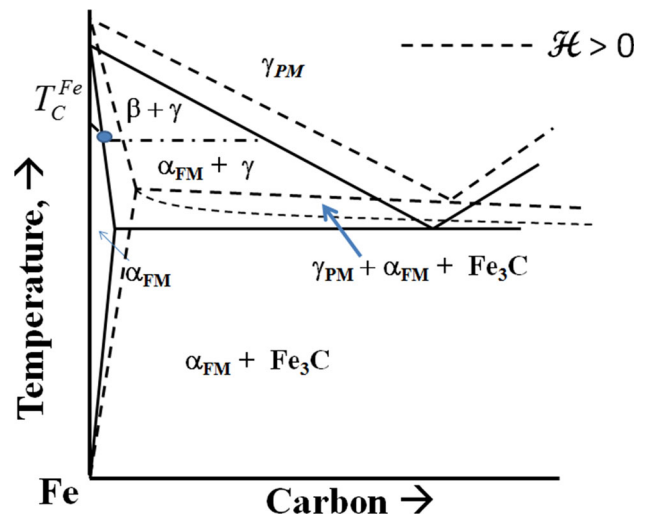


Fig. 19—A schematic of the Fe-C metastable phase diagram showing the effect of an applied magnetic field on the phase boundaries. An applied magnetic field always enlarges the region of stability of the phase or phases with the largest susceptibility. Note that the three-phase line for the reaction $\gamma \rightarrow \alpha_{FM} + Fe_3C$ is no longer a constant temperature invariant line since the applied external magnetic field increases the degrees of freedom in the system. The pressure is constant in the diagram. After Ref. [30].

IX. CONCLUSIONS

In this paper, some of the salient features of the phase boundaries (Curie Lines) of paramagnetic-to-ferromagnetic transformations have been presented. Important points include the following:

- (1) When the intensive magnetic field \mathcal{H} is present, the thermodynamic system (alloy) has an added degree of freedom.
- (2) The paramagnetic-to-ferromagnetic transformation need not follow the rules for the construction of phase diagrams containing first-order transformations.
- (3) The phase boundary between the paramagnetic phase and its conjugate ferromagnetic phase is not a coexistence curve: only the disordered paramagnetic phase is present on the boundary.
- (4) The phase boundaries of paramagnetic phases in phase diagram shift with the application of a magnetic field \mathcal{H} . The lines shift in such a way as to increase the region of stability of the phase with the higher magnetic susceptibility.
- (5) Equilibrium boundaries between two magnetic phases may follow the Gibbs Equilibrium Phase Rule.
- (6) Two or more higher-order or continuous transition curves may be present in some materials and their intersections produce an array of phase stability regions and transformations paths which must be carefully investigated. Bicritical, tricritical, and tetracritical intersections are discussed in the paper.
- (7) The application of an external magnetic field in combination with changes in temperature may produce regions of stability in the phase diagrams that are not present in the equilibrium diagram without the applied magnetic fields. This occurs because of the increase in the degree of freedom in the system with the application of the intensive magnetic field variable. This opens up the possibility of obtaining microstructures with metastable phases present when the magnetic fields are removed.

ACKNOWLEDGMENTS

I am very grateful to *ASM International* for the honor of naming me as the 2017 Edward DeMille Campbell Memorial Lecturer. I am thankful to my colleagues Professors William A. Soffa, T. B. Massalski, M. E. McHenry, and G-J Zhu for the many conversations on magnetic phase equilibria. Professor Soffa is also thanked for his helpful comments (and correction!) on an early draft of the paper. The many students in my graduate classes Magnetic Materials, Thermodynamics, and Phase Transformations of

Materials over the past few decades have stimulated my thinking on this topic. The National Science Foundation (NSF) is also thanked for continued support over the last several decades. Currently, Michael McHenry and I are supported through Grant DMR-1709247.

REFERENCES

1. W.A. Soffa and D.E. Laughlin: in *Physical Metallurgy*, D.E. Laughlin and K. Hono, eds., Elsevier, New York, 2014, vol. I, pp. 851–1019.
2. K. Honda and H. Takaki: *J. Iron Steel Inst.*, 1915, vol. 92, pp. 181–195 and Correspondence of A. McCance, pp. 196–98.
3. M. Cohen and J.M. Harris: in *Sorby Centennial Symposium*, AIME, 1963, pp. 209–33.
4. D.E. Laughlin: *J. Phase Equilib. Diffus.*, 2018, vol. 39, pp. 274–79, <https://doi.org/10.1007/s11669-018-0638-z>.
5. L.D. Landau and E.M. Lifshitz: *Statistical Physics*, Pergamon Press, London, 1980.
6. A.P. Cracknell: *Magnetism in Crystalline Materials*, Pergamon Press, London, 1975.
7. B.K. Vainshtein: *Modern Crystallography I*, Springer, Berlin, 1981.
8. S. Shaskolskaya: *Fundamentals of Crystal Physics*, Mir Publishers, Moscow, 1982.
9. L.A. Shuvalov: *Modern Crystallography IV*, Springer, Berlin, 1988.
10. Y. Shen and D.E. Laughlin: *Philos. Mag. Lett.*, 1990, vol. 62, pp. 187–93.
11. S.J. Joshua: *Symmetry Principles and Magnetic Symmetry in Solid State Physics*, Adam Hilger, Bristol, 1991.
12. D.E. Laughlin, M.A. Willard, and M.E. McHenry: in *Phase Transformations and Evolution in Materials*, P. Turchi and A. Gonis, eds., The Minerals, Metals and Materials Society, Pittsburgh, 2000, pp. 121–37.
13. W.H. Keesom and A.P. Keesom: *Proc. R. Acad. Amst.*, 1932, vol. 35, p. 736.
14. P. Ehrenfest: *Verhandlungen der Koninklijke Akademie van Wetenschappen, Amsterdam*, 1932, vol. 36, p. 153.
15. A.B. Pippard: *The Elements of Classical Thermodynamics*, Cambridge University Press, Cambridge, 1957, pp. 136–14.
16. D.R. Gaskell and D.E. Laughlin: *Introduction to the Thermodynamics of Materials*, CRC Press, Boca Raton, 2017, pp. 659–67.
17. D.E. Laughlin and W.A. Soffa: *Acta Mater.*, 2018, vol. 145, pp. 49–61.
18. T.B. Massalski and D.E. Laughlin: *CALPHAD*, 2009, vol. 33, pp. 3–7.
19. J.L. Meijering: *Philips Res. Rep.*, 1963, vol. 18, pp. 318–30.
20. T. Nishizawa, M. Hasebe, and M. Ko: *Acta Metall.*, 1979, vol. 21, pp. 817–28.
21. G. Inden: *Physica B, C*, 1981, vol. 103, pp. 82–100.
22. G. Inden: *Bull. Alloy Phase Diagr.*, 1982, vol. 2, pp. 412–22.
23. G. Inden: in *Atomic Ordering, Phase Transformations in Materials*, G. Kostorz, ed., VCH Publications, Inc., New York, 2001.
24. A.P. Miodownik: *Bull. Alloy Phase Diagr.*, 1982, vol. 2, pp. 406–12.
25. L.D. Landau: *JETP*, 1937, vol. 7, pp. 19ff, 627f.
26. S.M. Allen and J.W. Cahn: *Mater. Res. Soc. Symp. Proc.*, 1983, vol. 19, pp. 195–210.
27. S.M. Allen and J.W. Cahn: *Scripta Metall.*, 1976, vol. 10, pp. 451–54.
28. G. Schlatter and W. Pitsch: *Z. Metal.*, 1975, vol. 66, pp. 660–68.
29. D.E. Laughlin and W.A. Soffa: in *Physical Properties and Thermodynamic Behaviour of Minerals*, NATO ASI Series C, E.K.H. Salje, D. Reidel, eds., 1988, vol. 225, pp. 213–64.
30. R.A. Jaramillo, S.S. Babu, G.M. Ludtka, R.A. Kisner, J.B. Wilgen, G. Mackiewicz-Ludtka, D.M. Nicholson, S.M. Kelly, M. Muruganath, and H.K.D.H. Bhadeshia: *Scripta Mater.*, 2005, vol. 52, pp. 461–66.

31. H.D. Joo, J.K. Choi, S.U. Kim, N.S. Shin, and Y.M. Koo: *Metall. Mater. Trans. A*, 2004, vol. 35A, pp. 1663–68.
32. I.V. Gervasyeva, V.A. Milyutin, E. Beaugnon, V.V. Gubernatorov, and T.S. Sycheva: *Philos. Mag. Lett.*, 2016, vol. 96, pp. 287–93.
33. I.V. Gervasyeva, V.A. Milyutin, and E. Beaugnon: *Physica B*, 2017, vol. 524, pp. 11–16.
34. V.A. Milyutin and I.V. Gervasyeva: *Lett. Mater.*, 2018, vol. 8, pp. 59–65.

Publisher's Note Springer Nature remains neutral with regard to jurisdictional claims in published maps and institutional affiliations.